Ecological Questions 36 (2025) 3: 107–126 http://dx.doi.org/10.12775/EQ.2025.030

Multi-criteria decision modelling for forest fire risk mapping in protected areas of Mayurbhanj District, Odisha: A Case study in a geomorphologically diverse touristic landscape

Swati Sharma[1,*], Siddhartha S. Parasar[2], Kanwarpreet Singh[3]

[1] Division of Research and Development, Lovely Professional University, Jalandhar, India-144411
[2]Amity Institute of Geoinformatics and Remote Sensing, Amity University, India
[3]Department of Civil Engineering, Chandigarh University, Gharuan, Mohali, Punjab, India
*Corresponding Author e-mail: swati.9238@gmail.com

Received: 1 August 2025 / Accepted: 5 September 2025

Abstract. Forest fires are one of the most serious environmental disasters that endanger the natural forest ecosystem. Forest fire catastrophes have recently received a lot of attention because of their escalating numbers and the effects of global climate change. Recognizing fire occurrence and their patterns is important in identifying fire risks to mitigate the potential fire-prone areas surrounding human settlements and potential protected areas. Additionally, smoke emissions from fires endanger public health and natural systems, plus the added impact of natural triggers such as rainfall may cause debris floods or landslides initiated from the burnt areas. This study seeks to highlight burnt area mapping of the environmentally protected area of Mayurbhanj District, Odisha, India, which was devastated in the year 2021 due to a massive forest fire event. The main aim of this study was to create a map that would be a reliable risk indicator of forest fire zones in a defined region of interest, which is important and famous as a unique Geotourism and recreational destination. The study of the forest fire probability (risk zones) involved the investigation of an array of pertinent natural and geomorphological independent variables, such as vegetation type, climate, topography, road buffer, historical fire data, etc. Multi-criteria decision model (MCDM), i.e., analytic hierarchy processes (AHP) and Fuzzy Analytic Hierarchy Processes (FAHP) were used to comparatively assign weightage as per their influence on the prevailing fire risk. Results indicate that 1,058 km² (30.79% of the study area) is highly susceptible to wildfires, posing a significant threat to biodiversity. Satellite-derived fire risk indices and historical MODIS fire data effectively delineate high-risk zones after the severe 2021 wildfire, highlighting the urgent need for mitigation. By leveraging modelling and geospatial analytics, this study presents a scalable wildfire risk management approach, offering valuable insights for policymakers and disaster mitigation authorities in fire-prone landscapes of touristic importance.

Keywords: forest fire; MCDM; AHP-FAHP; protected areas; Simlipal Biosphere Reserve; risk assessment; geo-environmental hazard.

1. Introduction

Humans rely on forests as a key resource for numerous purposes, including recreation, clean air, firewood, natural raw materials, medicinal herbs, etc, and are an abode for millions of different types of plants and animal species. One of the main global threats to the natural forest system at present is the forest fire events globally that have exponentially increased over the past decade, leading to changes in their spatial coverage and affecting the natural climatic patterns, along with the hydrological networks (Dhar et al., 2023). According to a few studies, the intense heat and

dryness brought on by climate change are what set off wildfires in many parts of the world (Yue et al., 2013). Speaking in the Indian context, approximately 36% of the nation's forests are at risk of fire, with over 10% of them being extremely prone to fire, according to a recent forest survey of India (FSI) report [https://fsi.nic.in/forest-fire-activities]. Due to several interferences, which are natural and man-made fire events, have negatively impacted the forests' health, and they are unable to produce commodities and offer ecological services (Dhar et al., 2023 Tamrakar & Sharma, 2024). Ninety-eight million hectares of forest were destroyed by forest fires in 2015 on Earth as per the report by the Food and Agriculture Organisation, 2020. For woods that are prone to fire, continuous protection, observation, and mapping are essential (Chand et al., 2006). Bobsien and Hoffmann (1998) stated in their research that fire has a significant global, regional, and local influence on the economy, environment, and socio-culture. The processes part of cloud microphysics, precipitation, and atmospheric circulation can all be impacted by fire-related aerosol and their ability to increase cloud condensation nuclei (CCN) concentrations in the atmosphere by an order of magnitude (Andreae et al., 2004; Ramanathan et al., 2001). According to several experts, fire managers, and fire management organisations, climate change is seen more in longer fire seasons, with big to extremely large flames in the forest (Bowman et al., 2021; Jolly et al., 2015; Sankey et al., 2018).

Modern methods and tools are emphasized in forest fire prevention and for devising control plans to manage and avoid fire events. Numerous studies offer suggestions for the mapping, tracking, and prevention of forest fires using satellite remote sensing (Jain et al., 1996). Ahmad et al. (2018) and Potic et al. (2017) discovered that one effective method for determining the danger and trend of a forest fire is to use geospatial analytics using GIS and Remote Sensing, where satellite data can be used to identify forest fires in various land uses (Kaufman et al., 1998), and the remote sensing methods and Geographic Information System (GIS) are now frequently used globally to evaluate and forecast the frequency of fires (Abedi Gheshlaghi et al., 2020; Giglio et al., 2006; Roy et al., 2002; Oskouei et al., 2024). Any kind of disaster risk study requires an assessment of the integrated spatial-temporal pattern of hazardous natural events, yet this component is frequently overlooked, and the bulk of studies take these two dimensions into account independently (Loboda & Csiszar, 2007; Middendorp et al., 2013) where, especially for the forest fire risk studies, analyze the MODIS satellite data, which uses thermal and intermediate infrared bands that pinpoint the fire sites and detect thermal abnormalities with comparatively higher precision, with repeated cycles of observation over an area (Pereira et al., 2017; Roy et al., 2002). A "fire risk zone" is an area where there is a high probability of fires, considering the natural and anthropogenic factors, plus the past events that might harm the nearby areas (Erten et al., 2004; Jaiswal et al., 2002). To reduce the potential consequences of forest fires, a precise risk zone map is necessary (Jaiswal et al., 2002).

In India, forest fire events are usually recorded from mid-February till the end of June, and these occurrences have a significant effect on biodiversity, soil ecology, the environment, and human health in forest regions (Mutthulakshmi et al., 2020). Furthermore, a major factor in the rise in forest fire events in India, like in other countries, has been climate change, which includes less precipitation, rising temperatures, and an increase in the frequency of droughts (Keenan, 2015). Also, anthropogenic activities have contributed in the increasing number of forest fires (Simioni et al., 2020) and for this reason, creating fire risk maps early for the vulnerable and affected areas is essential for spotting future threats and their inevitable effects on the environment and societal infrastructure (Ghorbanzadeh et al., 2019). Additionally, forest fire risk maps are incredibly useful tools for lowering vulnerability and improving ecological risk in the decision-making process for working on the most essential parameter that triggers or enhances the fire event (Gong et al., 2022). Numerous conditioning factors for forest fires are mostly extracted from remote sensing (RS) techniques and processed by geographic information systems (GIS), which may help to create several of these risk maps (Lamat et al., 2021). Such analysis considers a wide range of factors, including temperature and humidity, alongside geo-environmental factors like elevation, aspect, slope angle, waterbody presence, and land use patterns etc. (Panwar & Chaudhary, 2019; Arca et al., 2020; Lamat et al., 2021; Moayedi & Khasmakhi, 2023; Tiwari et al., 2021; Shi et al., 2023; Nur et al., 2023 and Teke & Kavzoglu, 2025).

In this study, a protected forest cover in Mayurbhanj District, commonly known as Similipal Biosphere Reserve, in one of the eastern Indian states, Odisha (Fig. 1), is famous for its rich biodiversity and natural resources (Dash & Behera, 2018), has been investigated which has witnessed several forest fire events over a decade and the most powerful event that destroyed a large part of this area in the year 2021, which lasted for at least 2 weeks [https://www.thehindu.com/news/national/other-states/simlipal-park-fire-under-control-rainfall-helps/article34051180.ece]. Due to this catastrophe, there was extensive environmental damage and various faunal species were forced into nearby human habitations [https://www.indiatoday.in/india/story/habitat-burnt-in-simlipal-forest-fire-wild-animals-enter-human-areas-in-odisha-1777385–2021–03–09]. The factors causing and aggravating the occurrence of forest fires were rated and weighted as per their prevailing importance and extent in

the study area for which a subjective analytic technique for multi-criteria decision-model (MCDM) was used. In an integrated approach, Analytical Hierarchy Process (AHP) – Fuzzy AHP were leveraged to assign weights to hydro-geological and environmental factors, for ascertaining the most important causal component of forest fire in the study area, which can be mitigated and managed to restrict the fire events in the future. To delve further into the analysis, the factors were structured to get insight into the causes that contributed to the maximum risk of forest fires in previous years, as well as for which forest fire risk maps using the AHP-Fuzzy AHP approach were generated for the area of interest (AOI). The maps divided the study area based on their exposure to future risk levels, ranging from very low to very high likelihood of experiencing a forest fire.

This study provides a piece of relevant information for fire risk management and prevention by targeting the right type of causal factors for mapping fire zones with high-risk potential. The study also highlights the fuzzy approach to improve the decision-making process while rating the factors in the multi-criteria decision model, which has been validated using the ROC-AUC approach for analysing the success rate of the risk maps generated. Such a study can be the precursor to underscore the importance of targeting the burnt areas, which have high elevations and moderate to steep slopes, to assess the post-fire debris flow hazards based on rainfall threshold analysis.

2. Study Area

The region under study includes the Similipal Bio-Reserve in the protected regime of Mayurbhanj District in Odisha, India, covering an area of about 3,430 km^2. The area extends from 86°15'43"E – 22°04'39"N to 86°36'58"E – 21°01'21"N (Long-Lat) (Fig. 1) and falls under the boundaries of the state of Jharkhand and Odisha in India. The terrain elevation ranges from the highest point of 1,124 m and the lowest goes up to 21 m above the mean sea level. The annual rainfall varies from 1200mm to 2000mm, and the temperature ranges from 9°C to 35°C in the study area (Singha et al., 2024).

Forest fires are a consistent occurrence in this region, particularly in the initial four months of the year, i.e., from January to April. Among these months of the year, only one stands out, the month of March, as having the highest number of fire events. The past 12-year fire event data (MODIS Data) was analysed from the study area, which shows 2021

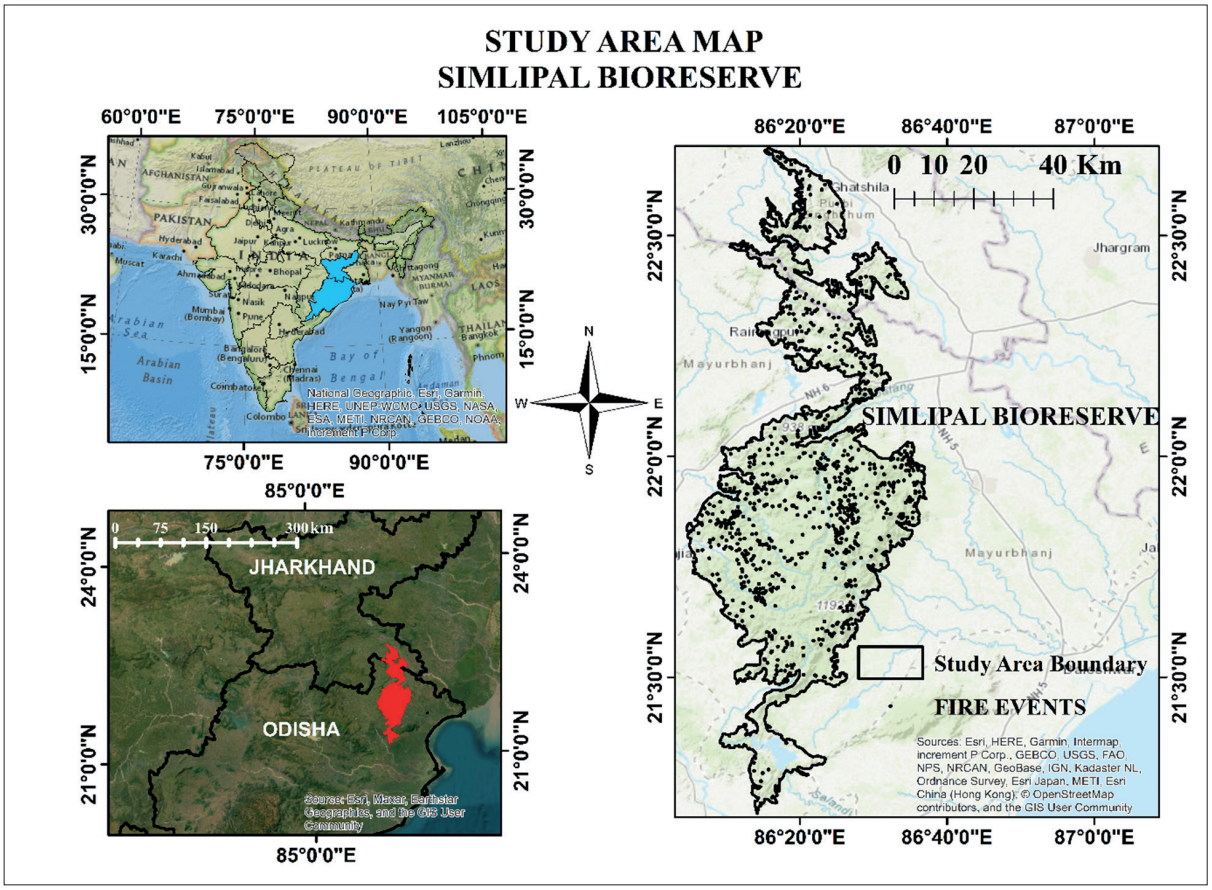

Figure 1. Study area location map

as the year with the highest number of fire occurrences. This dataset was revised for a confidence of more than 30% (Fig. 2), showing the trends of the fire event occurrences that remained the same with 2021 as the year of the highest recorded forest fires in the Similipal bio-reserve. Furthermore, the occurrence of most events of spring fires was observed for March for over a decade. The 2021 forest fires that occurred in the Similipal bio-reserve stand out as a very destructive event, ably proving the necessity and urgency of practical fire management and prevention approaches. The referred data, as shown in Figure 2, shows why this area was chosen for risk mapping and how this problem can aggravate other geological processes like debris flows, landslides, etc., in this region if precipitation occurs post-fire and can effectively destroy the natural habitat of various flora and fauna.

3. Methodology

To assess comprehensively the risk of forest fires, thematic maps of certain natural and anthropogenic factors were used to map their spatial variations in the study area and to rate them as per their impact on the prevailing fire occurrences. These maps therefore were strictly constructed for this specific study using the different software tools and data sources as mentioned in Table 1. The Array-5 satellite sensor in conjunction with the ALOS-PALSAR digital elevation model (DEM) with 12.5 m resolution was used to deliver in-depth topographical data. USGS Earth Explorer Landsat-8 data served as a valuable source of land cover information. To build on existing research the landforms and geological details were sourced from the Bhukosh link for obtaining geological and geomorphological data. With the help of ArcMap software, these maps were created at the required resolution and homogenised. The creation of thematic maps, such as LULC, NDVI, NDMI, road-to-fire distance buffer, LST, slope, aspect, and elevation maps contributed the information to comprehend the risk factors in a better recognized and organized manner.

The multi-criteria decision approach i.e. AHP (Analytic Hierarchy Process) was employed to allocate scores to the chosen thematic factors and their sub-classes as per their importance and relevance for causing the fire events in the study area which depicted the most important causal factors of forest fires that need to be managed for sustainable preservation of this protected area i.e. Similipal bio-reserve. AHP is useful for handling both quantitative and qualitative criteria in multi-criteria decision-making problems based on the judgments of decision makers, but many decision-making problems have fuzziness and vagueness, which can lead to decision makers' imprecise judgments in conventional AHP approaches (Bouyssou et al., 2000). In addition to the rating-weighting of the thematic factors through AHP, the criteria were fuzzified to remove any redundancies in the judgments while applying AHP-based decisions. The resulting AHP values (weights) were registered with the respective thematic maps and the weighted overlay was applied to extract the fire risk map. The weights obtained from applying the fuzzy analytical hierarchy process (FAHP) method were also used to generate another forest fire risk map. The resultant map's accuracies were based on the Area Under the Curve (AUC) method using the overlay with the past fire event data of the study area. Figure 3 presents the methodology used in this study.

It is the very basis of a reliable and scientifically strong system to evaluate the risk of wildfires using highly sophisticated remote sensing data coupled with an analytical approach. It enabled an understanding of the study area's present conditions and the application of specific forest improvement measures. This study has also highlighted the future risk toward the secondary geological hazards (debris flow, landslides) if triggered with heavy precipitation post a heavy fire event owing to the presence of steep slopes with high elevation in some parts of the study area.

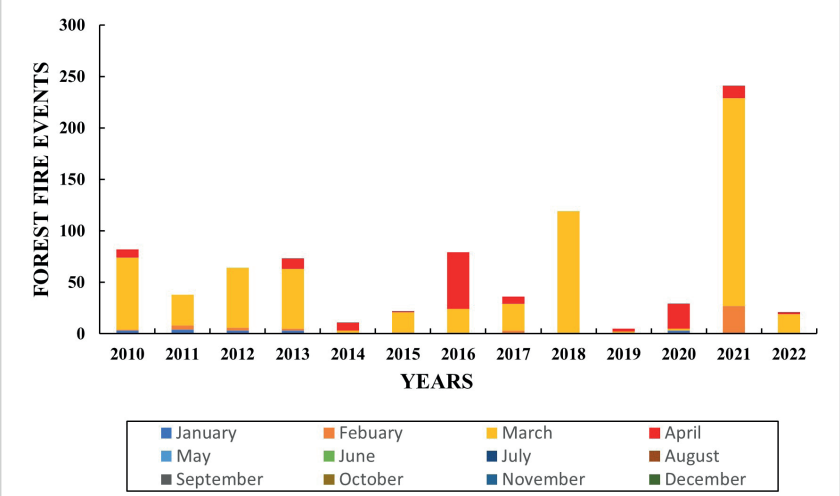

Figure 2. Forest Fire Trend 2010–2022 (confidence % > 30)

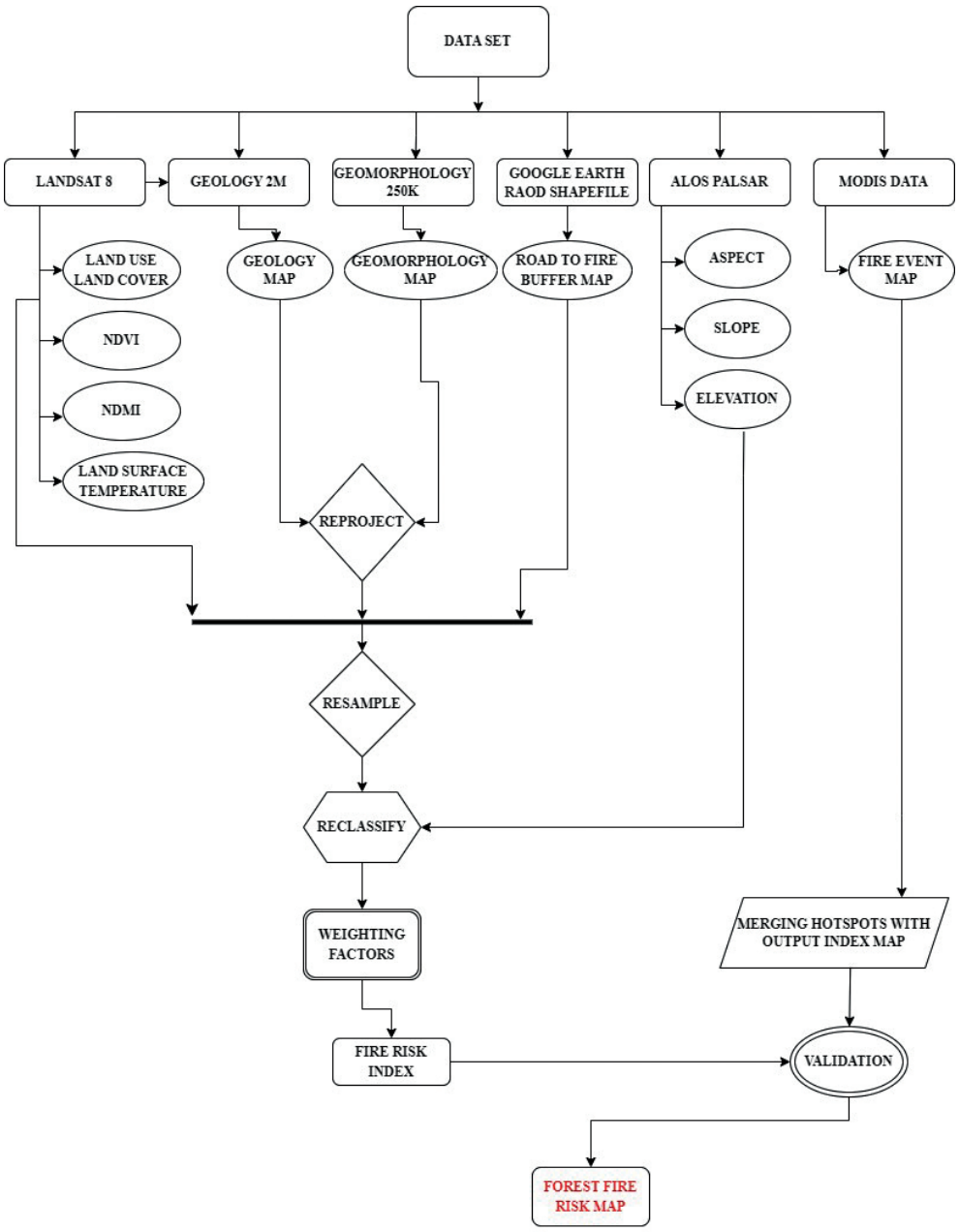

Figure 3. Shows the methodology adopted

Table 1. Data chard

S. NO.	Name of the data	File type	Type of data	Resolution	Layers extracted from the data	Source of the data
1.	LANDSAT 8	TIFF	Raster	30m	1. LAND USE LAND COVER MAP 2. NDVI MAP 3. NDMI MAP 4. LST MAP	https://earthexplorer.usgs.gov/
2.	MODIS DATA	SHP	Point		1. FIRE EVENT MAP	https://firms.modaps.eosdis.nasa.gov/download/
3.	ALOS PALSAR	TIFF	Raster	12.5 m	1. ELEVATION MAP 2. SLOPE MAP 3. ASPECT MAP	European Space Agency
4.	Geomorphology 250k	SHP	Feature	1:250000	1. GEOMORPHOLOGICAL MAP	https://bhukosh.gsi.gov.in/Bhukosh/
5.	Geology 2m	SHP	Feature	1:2000000	2. GEOLOGICAL MAP	https://bhukosh.gsi.gov.in/Bhukosh/
6.	Study area boundary	SHP	Polygon		1. STUDY AREA BOUNDARY	Google Earth Pro
7.	Google Earth road shapefile	SHP	Polyline		1. ROAD TO FIRE BUFFER MAP	Google Earth Pro

4. Data Processing, Results, and Discussion

4.1. Contributing Factor Maps

A. Land Use and Land Cover Map (LULC)

The term Land Use and Land Cover (LULC) refers to how land is used for agriculture, conservation, development, recreation, animal habitats, urban areas, or any other activity (Prakasam, 2010; Rawat & Kumar, 2015; Reis, 2008; Seyam et al., 2023). In this study, the LULC map (Figure 4(a)) indicated 7 land cover classes in Similipal bio-reserve, namely water bodies, vegetation cover, shrubs, low-lying vegetation, barren land, high relief area, and uncultivated Area. The map classes were further reclassified by applying AHP, giving vegetation cover the highest rank and water bodies the lowest, concerning the natural cause of fire activity. The forest fire point vector dataset from the year 2010 to 2022 was overlaid on the LULC map (Fig. 4), indicating fire events in various map classes.

B. Normalized Difference Vegetation Index Map (NDVI)

Kriegler et al. (1969) suggested a straightforward band transformation that produced a novel simplified picture known as the normalized difference vegetation index (NDVI) i.e. near-infrared (NIR) radiation minus red radiation divided by near-infrared radiation plus red radiation (equation 1) (Huang et al., 2021; Kriegler et al., 1969). NDVI values vary from –1 to 1, regardless of radiance, reflectance, or DN input. In general, its values are negative for water bodies, near zero for rocks, sands, or concrete surfaces, and positive for vegetation, such as crops, shrubs, grasses, and forests (Huang et al., 2021). The NDVI map (Figure 4(b)) in this study was reclassified into 5 classes applying AHP, namely very low, low, medium, high, and very high, with very high given the highest rank of 5 and very low given the lowest rank of 1, each class indicating the amount of vegetation in a particular area. The fire events from 2010–2022 are overlaid on the NDVI map, and it indicates how the areas with high to very high vegetation cover have encountered more forest fires than those areas having very low or low vegetation cover. In this study, NDVI is given the highest priority rather than LST as land surface temperature greatly increases post-fire events (Vlassova et al., 2014), and the temperature difference between the unburned areas and burned areas was on average 7.6°C.

Mathematically,

$$NDVI = \frac{NIR - red}{NIR + red} \qquad \text{eq. 1}$$

NDVI = Normalized Difference Vegetation Index,
NIR = Near Infrared,
Red = Red Band.

C. Normalized Difference Moisture Index Map (NDMI)

The structure of the plants is inextricably linked to the moisture content that exists within them (Basak et al., 2023). If an area has high moisture content, it suggests healthy trees and more vegetation, thus being fuel for a forest fire. The value of NDMI is between +1 to -1 (Taloor et al., 2021) (equation 2). The NDMI map (Figure 4(c)) generated for this study was reclassified into 5 classes applying AHP, namely very low, low, medium, high, and very high, depending upon the moisture index. Very high class was given the highest rank of 5 and very low was given the lowest rank of 1. The forest fire data from 2010–2022 were overlaid with the NDMI map, which showed that the areas having very high to high moisture content experienced maximum fire events than the areas with low to very low moisture content.

Mthematically,

$$NDMI = \frac{NIR - SWIR}{NIR + SWIR} \qquad \text{eq. 2}$$

NDMI = Normalized Difference Moisture Index,
NIR = Near Infrared,
SWIR = *Short Wave Infrared.*

D. Land Surface Temperature Map (LST)

An LST map indicates the temperature of an item within a pixel, which can include various land cover categories (Taloor et al., 2021), and in the present study area (Fig. 5(a)) LST shows a maximum of 63.28°F, which is 17.37°C, and a minimum of 51.20°F, which is equal to 10.67°C. The forest fire events data were overlaid on the LST map, and it indicates that the areas having lower land surface temperature are experiencing more forest fire events. This comes from a scientific understanding that areas with dense vegetation tend to have a cooling effect on the land, whereas areas with very little vegetation or that are barren absorb more solar energy and lack the cooling effect, resulting in higher surface temperature (Vlassova et al., 2014). The LST map was further reclassified applying AHP into 5 classes, namely: very high, high, medium, low, and very low, giving the very low LST class the highest rank and very high LST the lowest rank. The process to find the LST of an area from Landsat 8 imagery is given below (equations 3, 4, 5, 6, 7 and 8):

Step 1. Top of Atmosphere (TOA) Radiance:

$$TOA = ML * Qcal + AL \qquad \textit{eq. 3}$$

where,
TOA = Top of Atmosphere Radiance,
ML = Radiance Multiband (Band 10),
AL = Radiance Add Band (Band 10),
Qcal = Band 10.

Step 2: Brightness Temperature (BT):

$$BT = K_2/ln\ (K_1/TOA + 1) - 272.15 \qquad eq.\ 4$$

where,
BT = Brightness temperature,
TOA = Top of Atmosphere,
$K_1 = K_1$ constant Band (Band 10),
$K_2 = K_2$ constant Band (Band 10).

Step 3: Normalized Difference Vegetation Index (*NDVI*):

$$NDVI = (NIR - Red)/(NIR + Red) \qquad eq.\ 5$$

where,
NDVI = Normalized Difference Vegetation Index,
NIR = Near Infrared,
Red = Reb Band.

Step 4: Proportion of vegetation (PV):

$$PV=\{(NDVI\text{-}NDVImin)/(NDVImax+NDVImin)\}\text{^}2 \qquad eq.\ 6$$

where,
PV = Proportion of vegetation,
NDVI = Normalized Difference Vegetation Index,
$NDVI_{min}$ = Minimum value of NDVI,
$NDVI_{max}$ = Maximum value of NDVI.

Step 5: Emissivity

$$E = 0.004 * PV + 0.986 \qquad eq.\ 7$$

where,
E = Emissivity,
PV = Proportion of Vegetation.

Step 6: Land Surface Temperature (LST)

$$LST = BT/(1+(\lambda * BT/C\text{^}2\ ) * ln\ (E)) \qquad eq.\ 8$$

where,
LST = Land Surface Temperature,
BT = Brightness Temperature,
$\lambda = 10.8$
C^2 = 14388
E = Emissivity.

E. Road Buffer Map

Identifying the distance of past fire events to nearby roads in a study area might help identify potential fire and high-risk regions for human activities (Chuvieco & Congleton, 1989). For this study, the distance for the road buffer was taken as 1 km, 2 km, 5 km, 8 km, 10 km, 12 km, 15 km, 18 km, 20 km, 22 km, 25 km, and 28 km, keeping in view the nearest distance to the fire event in the past. From the road buffer map (Fig. 5(b)) it can be inferred that many fire events took place within the range of 1 km to 5 km from the road in the period of 2010–2022, giving a rough idea of anthropogenic influence in causing forest fires. This map was reclassified applying AHP, giving 1 km the highest rank and eventually 28 km the lowest in terms of the risk to fire activity.

F. Geology Map

The Geological data was obtained from the Bhukosh website [https://bhukosh.gsi.gov.in/Bhukosh/Public]. The map was generated by further extracting the information according to the AOI using the clip feature. Since the geological map was in shapefile format of scale 1:2000000, firstly it was reprojected according to the coordinate system and then was converted using the conversion tool from feature to raster format. The geological map (Fig. 6(a)) shows 17 formation details, and they were reclassified again by applying AHP. Since geological formations do not have much of an influence in causing forest fires so, the 17 classes were reclassed according to the number of fire events that took place over each formation in the past 12 years giving broad information about the classes more prone and less prone as per the spatial distribution of the fire activities. The geology map (Fig. 9) was thus generated, and the forest fire events were overlaid on it.

G .Geomorphology Map

The Geomorphological data was obtained from the Bhukosh website [https://bhukosh.gsi.gov.in/Bhukosh/Public] and the map was generated by the same process used to generate the geological map. The initial shapefile was of scale 1:250000 and the thematic map (Fig. 6(b)) shows 9 geomorphological features classified applying AHP, giving the highest rank to highly dissected Hills and valleys, and the lowest rank to Water Bodies.

H. Elevation Map

The Elevation map was generated using the ALOS-PALSAR digital elevation model (DEM) of 12.5 m resolution. The elevation map (Fig. 7(a)) shows a maximum elevation point of 1,124 meters above mean sea level. The map was further reclassified applying AHP into 5 elevation classes. The forest fire events data from 2010–2022 was overlaid on the elevation map, giving us a clear view of how places according to their elevation were affected by the forest fire events.

I. Aspect Map

There are different definitions of aspect in literature, which represent the maximum slope direction of the land surface

(Tanoli et al., 2017); or for any point, the aspect represents the direction of the maximum variation of the degree of the height value (Chen et al., 2013). It also indicates the maximum altitude change towards the downward slope direction (Bourenane et al., 2015; Zhuang et al., 2015). The clockwise sides of a slope between 0° and 360°, is measured in degrees from the North, are referred to as the aspect (Hadji et al., 2016; Lee, 2005). The aspect typically spans from 0° to 360° and is split into groups at 45°, the directions are North, Northeast, East, Southeast, South, Southwest, West, and Northwest (Fig. 7(b)) in a clockwise manner (Cellek, 2021; Geiger et al., 2009; Warren, 2008; Singh, 2018).

J. Slope Map

The slope map was also generated using the ALOS PALSAR digital elevation model (DEM) of 12.5 m resolution. The slope map in Figure 7(c) was reclassified using AHP into 5 classes: very low, low, medium, high, and very high. The classes were ranked by giving the highest rank to a very low inclined slope, and the lowest rank to a very high inclined slope. With a high degree of slope, the possibility of slope instability increases, and resins, oils, and fats held in plants and debris are vaporized, much like at high temperatures experienced during a fire. Both the soil and the atmosphere are exposed to these vapours; condensing into the lower, colder soil under the surface, the soil vapours reorganize into the hydrophobic layer, which is a layer that repels water [https://www.csus.edu/indiv/k/kusnickj/geology140/fire.html]. Changes in vegetation, surface cover conditions, and hydrological processes following a forest fire can raise the likelihood and severity of slope instability events, which can have long-term effects on the regions in front of or above the slopes. The first four to six months following the fire are often the most vulnerable due to the possibility of heavy rainfall during the season and the lack of regrowth of vegetation (Nunes & Lourenço, 2017; Arujo et al., 2020) and rainfall can often act as the primary cause of slope instability events, according to Esteves et al. (2012), Zêzere et al. (2015), and Mahajan et al. (2022).

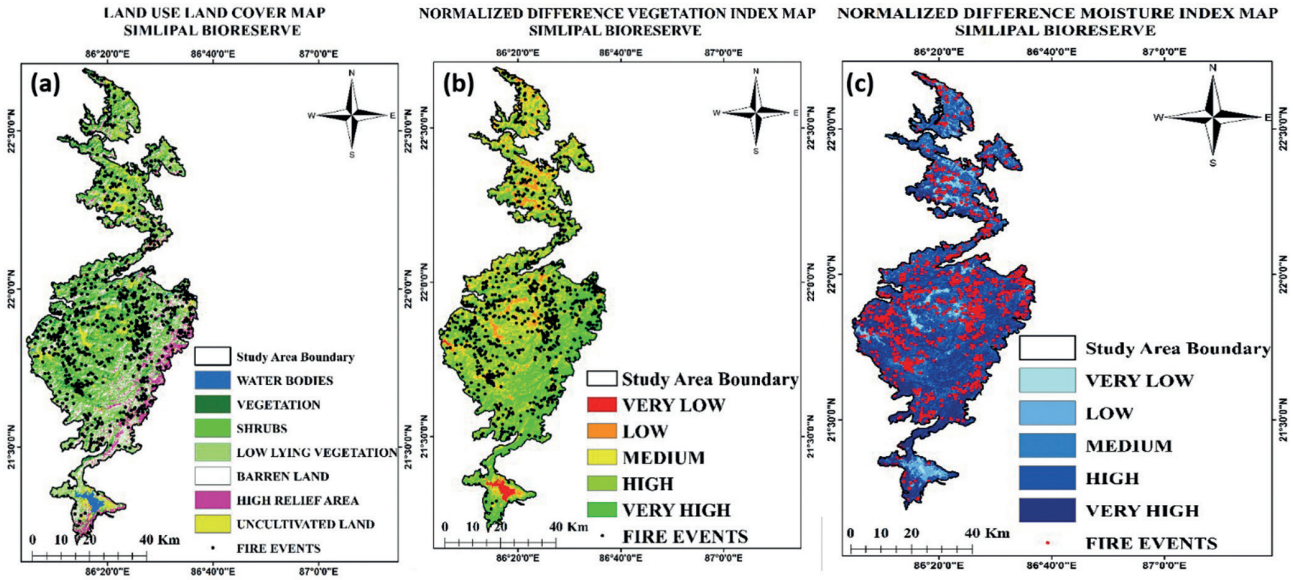

Figure 4. (a) Land Use Land Cover Map, (b) Normalized Difference Vegetation Index Map & (c) Normalized Difference Moisture Index Map depicting moisture-related vegetation conditions. Fire event points (2010–2022) are overlaid with thematic classes

Table 2. Continuous data Classification for NDVI, NDMI, LST, Slope, and Elevation Maps

Map Sub-Class	NDVI Class Value	NDMI Class Values	LST Class Values (˚F)	Slope Class Values	Elevation Class Value (m)
Very Low	0.034–0.10	0.167–0.029	61.08–64.09	0–10˚	21–230
Low	0.109–0.243	0.029–0.089	64.09–65.22	10˚- 20˚	230–419
Medium	0.243–0.298	0.089–0.136	65.222–66.40	20˚ – 30˚	419–616
High	0.298–0.344	0.136–0.167	66.40–67.71	30˚ – 40˚	616–791
Very High	0.3445–0.744	0.167–0.272	67.71–72.19	>40˚	791–1124

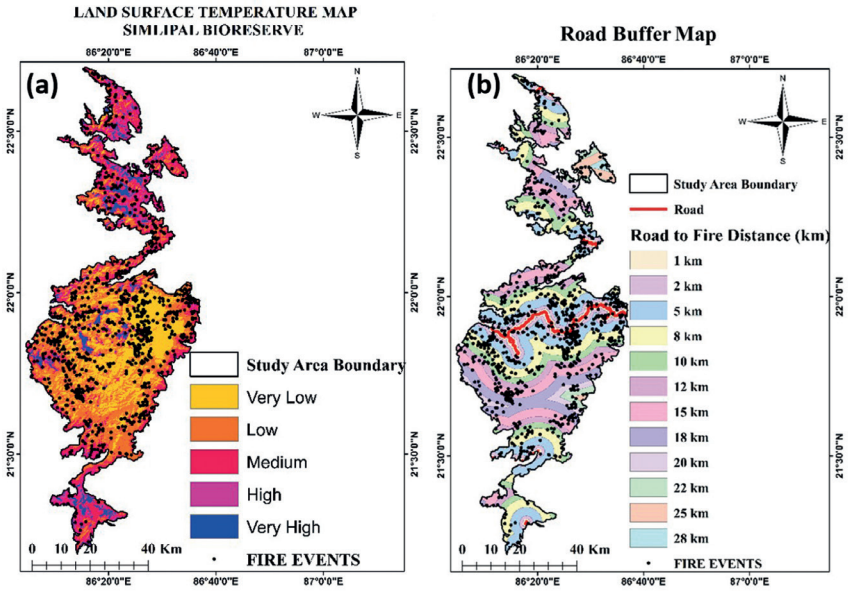

➤ **Figure 5.** (a) Land Surface Temperature (SAT) Map indicating surface thermal variability (b) Road Buffer Map illustrating anthropogenic influence zones

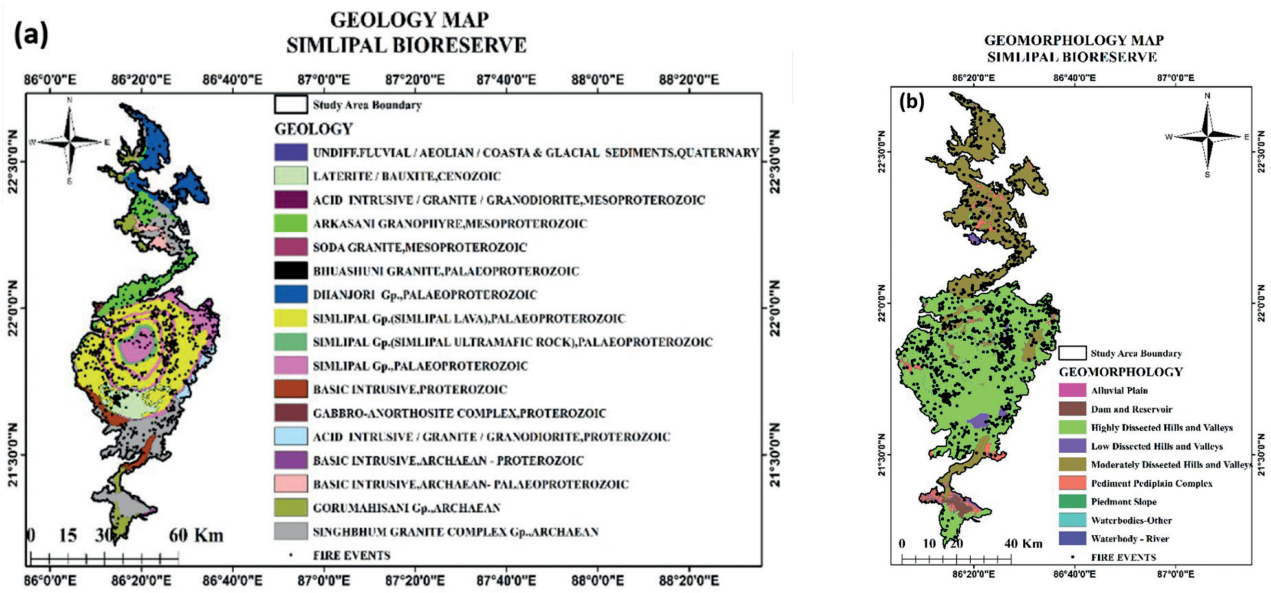

➤ **Figure 6.** (a) Geology Map (b) Geomorphology Map highlighting landform classes such as dissected hills, valleys, and plains, overlaid with past fire locations

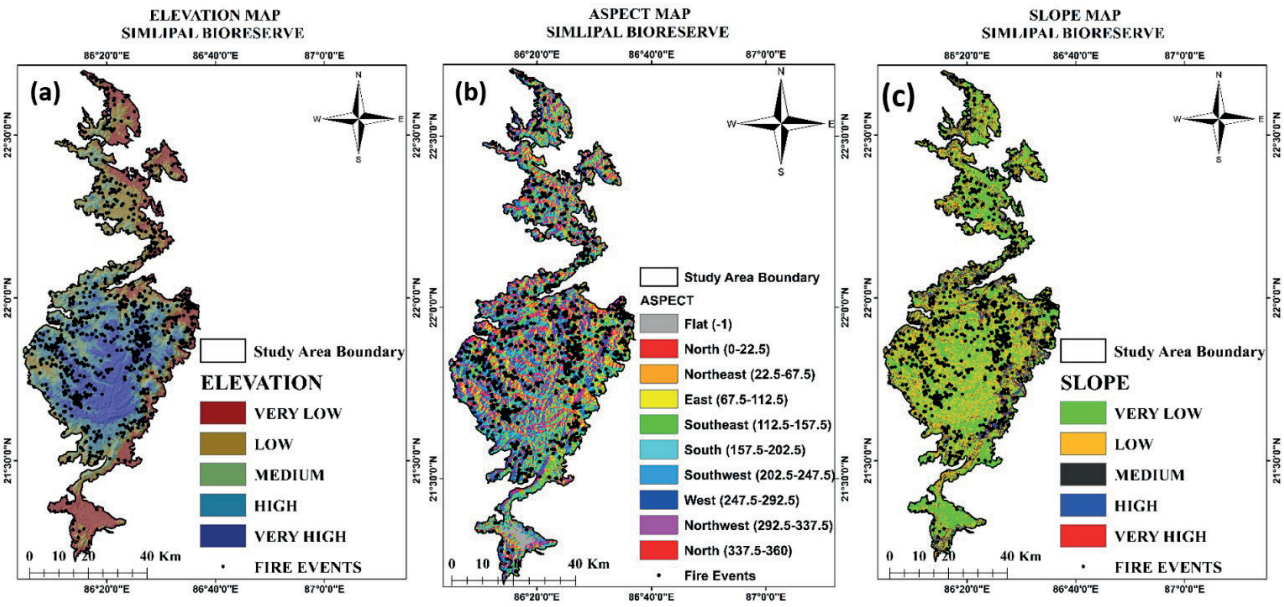

Figure 7. (a) Elevation Map derived from ALOS-PALSAR DEM with fire events (b) Aspect Map showing slope orientation classes with fire events (c) Slope Map with fire events to depict susceptibility trends

4.2. Models Applied

A. Analytical Hierarchy Process

In this study, the forest fire risk map (Fig. 8) was firstly generated by combining all the factor maps namely: LULC map (Fig. 4a), NDVI map (Fig. 4b), NDMI map (Fig. 4c), LST map (Fig. 5a), Road to fire distance map (Fig. 5b), Geology Map (Fig. 6a), Geomorphology map (Fig. 6b), Elevation map (Fig. 7a), Aspect map (Fig. 7b) and Slope map (Fig. 7c). Each factor and its impact on causing the forest fire was weighted and categorized, and appropriate weights were assigned to each sub-class in the factor maps with certain class values (Table 2). A higher number indicates that the factor is more relevant to causing fires in a region (Pandey & Ghosh, 2018). The weights were assigned using AHP, considering the past literature, general characteristics of the study area, and the general relation between factors and fire activity based on previous studies in this field.

The AHP technique is one of the most used MCDMs (Rahmati et al., 2015) and in many regions of the world, AHP and geospatial techniques have been effectively used to identify fire risk zones (Chavan et al., 2012; Chowdhury & Hassan, 2013, 2015; Matin et al., 2017; Nuthammachot & Stratoulias, 2021; Pourghasemi et al., 2016; Van Hoang et al., 2020). When a decision maker must choose amongst several criteria, the AHP approach ranks the choices and helps them choose the best one (Özdağoğlu & Özdağoğlu, 2007). In AHP, preferences for alternatives are derived through pairwise comparisons which involve comparing two choices based on a single criterion and indicating a preferred option. The 1–9 scale is the typical preference scale (Table 3) used for AHP; it falls between "equal importance" and "extreme importance". Within the pairwise comparison matrix, a value of 9 signifies a factor that is significantly more important than the other, a value of 1/9 denotes a component that is significantly less important than the other, and a value of 1 shows a factor of equal significance (Özdağoğlu & Özdağoğlu, 2007; Sarkis & Talluri, 2004). Intermediate values such as 2, 4, 6, and 8 indicate intermediate importance.

Table 3. Relative Importance of the Scale from 1–9

Scale	1	3	5	7	9
Importance	Equal Importance	Moderate Importance	Strong Importance	Very Strong Importance	Extreme Importance

The values 2, 4, 6, and 8 show indecisiveness between the factors.

Now, the consistency ratio value must be below 0.01; otherwise, the comparison matrix must be re-examined, or it can be considered inconsistent. The consistency ratio (C.R.) is obtained by comparing the consistency index (C.I.) with the appropriate set of numbers, each of which is an average of the random index (R.I.) of a randomly generated reciprocal matrix using the scale l/9, l/8, 1, 8, 9 to see if it is about 0.10 or less. If it is not less than 0.10, the problem is revised for the judgments (Saaty, 1987).

The formula for CR is:

$$CR = CI/RI \qquad \text{eq. 9}$$

CI is the consistency index and is mathematically obtained by:

$$CI = (\Delta max - n)/(n - 1) \qquad \text{eq. 10}$$

R.I is the random consistency index and the values for 10 factors (Saaty, 1987) are given below in Table 4.

Table 4. R.I table for 10 factors

n	1	2	3	4	5	6	7	8	9	10
Random Consistency Index (R.I)	0	0	0.58	0.90	1.12	1.24	1.32	1.41	1.45	1.49

The resultant consistency ratio (CR) for contributing factors came out to be 0.097 based on Table 5 and the

Table 5. Comparison matrix for the factor used in the study

Factors	LULC	NDVI	NDMI	LST	ROAD TO FIRE	GEOLOGY	GEOMORPHOLOGY	ELEVATION	ASPECT	SLOPE	WEIGHTAGE	RANK
LULC	1	1/6	1/5	1/3	7	8	7	5	1/3	3	**0.08**	5
NDVI	6	1	3	4	9	9	9	7	5	7	**0.318**	1
NDMI	5	1/3	1	2	8	9	7	7	3	5	**0.208**	2
LST	3	1/4	1/2	1	8	9	7	7	2	5	**0.143**	3
ROAD TO FIRE	1/7	1/9	1/8	1/8	1	1	1/3	1/3	1/8	1/6	**0.014**	9
GEOLOGY	1/8	1/9	1/9	1/9	1	1	½	1/4	1/8	1/7	**0.013**	10
GEOMORPHOLOGY	1/7	1/9	1/7	1/7	3	2	1	1/3	1/7	1/5	**0.02**	8
ELEVATION	1/5	1/7	1/7	1/7	3	4	3	1	1/7	1/3	**0.029**	7
ASPECT	3	1/5	1/3	1/2	8	8	7	7	1	5	**0.186**	4
SLOPE	1/3	1/7	1/5	1/5	6	7	5	3	1/5	1	**0.052**	6

principal Eigen Value The resultant consistency ratio (CR) for contributing factors came out to be 0.097 based on Table 5 and the principal Eigen Value resulted in 11.301. The subclasses of each factor map were also rated (Appendix 1) to give them new values according to their relevance in causing the fire events; hence, the judgements were used to generate the forest fire risk map (Fig. 8), by following the weighted overlay approach, combining the factor maps with the already assigned weights.

The resultant forest fire risk map was classified into 5 classes: Very High, High, Medium, Low, and Very Low (Table 6). The Principal Eigen Value of the pair-wise comparison AHP matrix of the forest fire risk index map is 5.315, with a consistency ratio value of 0.07.

Table 6 shows the factors that were selected for this study, including the sub-classes in each factor and how AHP was applied for comparative matrix generation. The principal eigenvalue and also the CR value of the individual factors are given (Appendix 1). In Land Use Land Cover (LULC), the priority was from highest to lowest as vegetation > Low Lying Vegetation > Shrubs > High Relief Area > Uncultivated Land > Barren Land > Water Bodies. Vegetation gets the highest priority in LULC as the presence of vegetation can initiate fire and provide the ground for the fire to grow and create devastating consequences. Water body on the other hand, because of its inability to catch fire is given the lowest priority, as the presence of water can put off the fire and will never allow the fire to grow. In the Normalized Difference Vegetation Index (NDVI), the areas with very high vegetation cover are given the highest priority as vegetation provides ground and accessories for the fire to initiate and spread. In the Normalized Difference Moisture Index (NDMI), the areas with very high moisture content indicate the presence of very high vegetation resulting in giving us the highest priority to areas indicating very high moisture content. Vegetations have a cooling effect on the ground leading to lowering the temperature of the surface, whereas areas with very low to zero vegetation show higher surface temperature, as the soil absorbs more heat energy coming from the sun, hence in the land Surface Temperature factor, the areas with very low to low surface temperatures are given high priority than the areas with high surface temperature. In the Road to Fire distance factor, the areas in close proximity to the road are given higher priority as vegetation near such roads is in constant danger of getting ignited knowingly or unknowingly due to anthropogenic factors or actions. Hence several fire events occurred between 1 to 5 km from the road. In Geology, there are a total of 17 subclasses, out of which Similipal Gp. (Similipal lava), The Palaeo-Proterozoic formation is given the highest priority as this formation has encountered fire events ranging between the year 2010 – 2022, and the lowest priority to Basic Intrusive, Archaean- Palaeo-Proterozoic formation. In geomorphology, the highest priority was given to Highly Dissected Hills and Valleys, as due to their slope dead leaves and branches could be found acting as fuel to the fire, the slope helps the fire to spread, and due to its dissected terrain, the wind pattern gets unpredictable, results in aiding the fire, wind patterns keep changing in such terrains which makes it very hard to contain the fire. Hence, the highest priority is given to highly dissected hills and valleys. And the lowest priority is given to water bodies. In case of elevation, the highest priority was given to high to medium elevation, because this study has experienced a lot of fire events in areas from high to medium elevation in the past. Aspect plays an important role in forest fire, and since the area of study is in the northern hemisphere, the south-facing slopes were given the highest priority, and the priority scale was South > East > West > North > Flat. For the slope factor, the highest priority was given to areas with very low to low inclined slopes. Looking through the historic fire event data from 2010 – 2022 and overlaying it over the slope map, it can be concluded that in the AOI, areas with very low to low slope conditions have experienced a higher amount of forest fire events. Hence, the priority was given to areas with low to very low slope conditions.

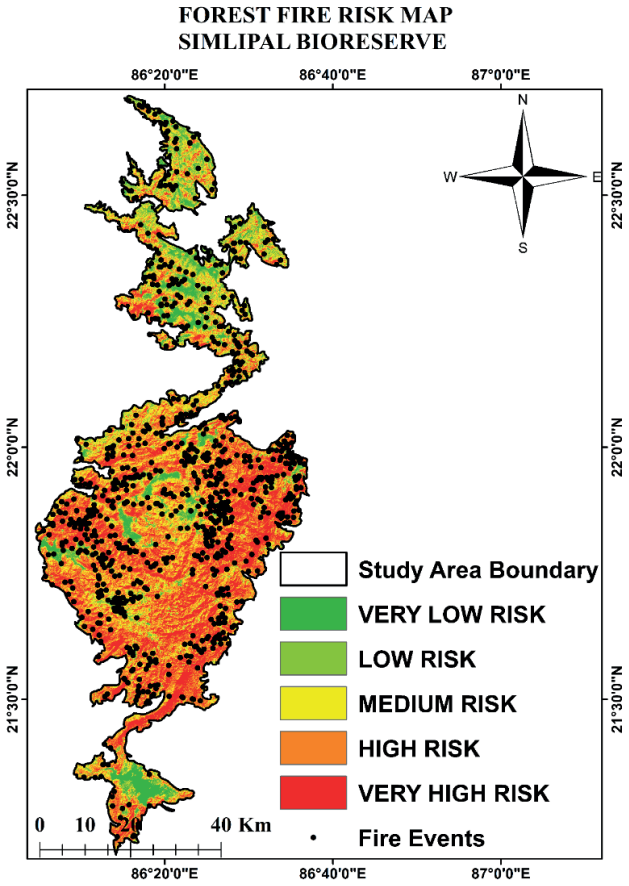

Figure 8. Forest fire risk map of Similipal Bio-reserve using the AHP model, classifying the area into very low to very high susceptibility zones

Table 6. Comparison matrix of Forest Fire Risk Map classes

Factors	Very High	High	Medium	Low	Very Low	Weightage	Rank
Very High	1	2	5	9	9	0.0463	1
High	1/2	1	5	7	9	0.337	2
Medium	1/5	1/5	1	3	7	0.12	3
Low	1/9	1/7	1/3	1	3	0.052	4
Very Low	1/9	1/9	1/7	1/3	1	0.029	5

B. Fuzzy Analytical Hierarchy Process (FAHP)

It is possible to think of the fuzzy AHP methodology as an improved analytical technique that evolved from the conventional AHP (Bouyssou et al., 2000). Although AHP is useful for handling both quantitative and qualitative criteria of multi-criteria decision-making problems based on the judgments of decision makers, many decision-making problems have fuzziness and vagueness, which can lead to decision makers' imprecise judgments in conventional AHP approaches (Özdağoğlu & Özdağoğlu, 2007). As a result, a large body of research has demonstrated that, in comparison to classic AHP approaches, fuzzy AHP provides a comparatively more adequate description of these types of decision-making processes. Fuzzy AHP is an extension of Saaty's theory (Boender et al., 1989; Buckley, 1985a, b; Lootsma, 2013; Ribeiro, 1996; Van Laarhoven & Pedrycz, 1983). In this study as well, the Fuzzy-AHP method was applied, and changes were observed in the weightage (Table 7) given to each factor in the simple AHP model.

After creating this table calculation for the Fuzzy geometric mean values were calculated (Table 8). Mathematically, it can be calculated using the following formula:

Fuzzy Geometric mean value (Ai, Bi, Ci) =
$(a1 * a2 * a3 \ldots an)^{\frac{1}{n}}, (b1*b2*b3 \ldots bn)^{\frac{1}{n}}, (c1 * c2 * c3 \ldots cn)^{\frac{1}{n}}$ eq. 11

Here,
n = no. of factors,
and a1, a2, a3,…., b1, b2 b3….., c1,c2, c3…. indicates the values given to each factor.

Table 8. Fuzzy geometric mean Values

Factors	Fuzzy GM values (Ai, Bi, Ci)
LULC	(1.1, 1.35, 1.67)
NDVI	(4.46, 5.14, 5.74)
NDMI	(2.66, 3.34, 4.02)
LST	(2.03, 2.58, 3.10)
Road to Fire Distance	(0.21, 0.23, 0.27)
GEOLOGY	(0.20, 0.22, 0.26)
GEOMORPHOLOGY	(0.27, 0.33, 0.40)
ELEVATION	(0.4, 0.5, 0.6)
ASPECT	(1.68, 2.08, 2.62)
SLOPE	(0.7, 0.86, 1.05)

Now the fuzzy weights of each factor (table 9) are given by:

$$Fuzzy\ weight\ (A, B, C) = \left(\frac{Ai}{\sum_{i=1}^{n} Ci}\right), \left(\frac{Bi}{\sum_{i=1}^{n} Bi}\right), \left(\frac{Ci}{\sum_{i=1}^{n} Ai}\right) \quad \text{eq.12}$$

where Ai, Bi, and Ci are individual Fuzzy GM values of the factors,
and n = no. of factors.

Table 9. Fuzzy Weights

Factors	Fuzzy Weights (A, B, C)
LULC	(0.055, 0.081, 0.1219)
NDVI	(0.233, 0.3084, 0.419)
NDMI	(0.133, 0.2004, 0.2934)
LST	(0.1015, 0.1548, 0.2263)
Road to Fire Distance	(0.0105, 0.0138, 0.0197)
GEOLOGY	(0.01, 0.0132, 0.0189)
GEOMORPHOLOGY	(0.0135, 0.0198, 0.0292)
ELEVATION	(0.02, 0.03, 0.0438)
ASPECT	(0.084, 0.1248, 0.1912)
SLOPE	(0.035, 0.0516, 0.0766)

Now the weights of each factor were calculated (Table 10) using the given formula:

$$Weights\ (Wi) = \frac{A+B+C}{3} \quad \text{eq. 13}$$

Table 7. Fuzzy AHP table

FACTORS	LULC	NDVI	NDMI	LST	ROAD TO FIRE	GEO-LOGY	GEOMOR-PHOLOGY	ELEVATION	ASPECT	SLOPE
LULC	(1,1,1)	(1/7,1/6,1/5)	(1/6,1/5,1/4)	(1/4,1/3,1/2)	(6,7,8)	(7,8,9)	(6,7,8)	(4,5,6)	(1/4,1/3,1/2)	(2,3,4)
NDVI	(5,6,7)	(1,1,1)	(2,3,4)	(3,4,5)	(9,9,9)	(9,9,9)	(9,9,9)	(6,7,8)	(4,5,6)	(6,7,8)
NDMI	(4,5,6)	(1/4,1/3,1/2)	(1,1,1)	(1,2,3)	(7,8,9)	(9,9,9)	(6,7,8)	(6,7,8)	(2,3,4)	(4,5,6)
LST	(2,3,4)	(1/5,1/4,1/3)	(1/3,1/2,1)	(1,1,1)	(7,8,9)	(9,9,9)	(6,7,8)	(6,7,8)	(1,2,3)	(4,5,6)
ROAD TO FIRE	(1/8,1/7,1/6)	(1/9,1/9,1/9)	(1/9,1/8,1/7)	(1/9,1/8,1/7)	(1,1,1)	(1,1,1)	(1/4,1/3,1/2)	(1/4,1/3,1/2)	(1/9,1/8,1/7)	(1/7,1/6,1/5)
GEOLOGY	(1/9,1/8,1/7)	(1/9,1/9,1/9)	(1/9,1/9,1/9)	(1/9,1/9,1/9)	(1,1,1)	(1,1,1)	(1/3,1/2,1)	(1/5,1/4,1/3)	(1/9,1/8,1/7)	(1/8,1/7,1/6)
GEOMOR-PHOLOGY	(1/8,1/7,1/6)	(1/9,1/9,1/9)	(1/8,1/7,1/6)	(1/8,1/7,1/6)	(2,3,4)	(1,2,3)	(1,1,1)	(1/4,1/3,1/2)	(1/8,1/7,1/6)	(1/6,1/5,1/4)
ELEVATION	(1/6,1/5,1/4)	(1/8,1/7,1/6)	(1/8,1/7,1/6)	(1/8,1/7,1/6)	(2,3,4)	(3,4,5)	(2,3,4)	(1,1,1)	(1/8,1/7,1/6)	(1/4,1/3,1/2)
ASPECT	(2,3,4)	(1/6,1/5,1/4)	(1/4,1/3,1/2)	(1/3,1/2,1)	(7,8,9)	(7,8,9)	(6,7,8)	(6,7,8)	(1,1,1)	(4,5,6)
SLOPE	(1/4,1/3,1/2)	(1/8,1/7,1/6)	(1/6,1/5,1/4)	(1/6,1/5,1/4)	(5,6,7)	(6,7,8)	(4,5,6)	(2,3,4)	(1/6,1/5,1/4)	(1,1,1)

Table 10. Weightage table

Factors	Weights (Wi)
LULC	0.086
NDVI	0.317
NDMI	0.209
LST	0.161
Road to Fire Distance	0.0146
GEOLOGY	0.014
GEOMORPHOLOGY	0.021
ELEVATION	0.031
ASPECT	0.133
SLOPE	0.054

Now all the weights were added and checked if it is = 1. Therefore, $\sum_{i=1}^{n} Wi$ gave a value of 1.0406 which is greater than 1 so the Normalized weights were again calculated (Table 11), mathematically which can be obtained by:

$$Normalized\ Weights\ (W) = \frac{Wi}{\sum_{i=1}^{n} Wi} \qquad \text{eq. 14}$$

Table 11. Normalized Weight Table

Factors	Normalized Weights (W)
LULC	0.082
NDVI	0.305
NDMI	0.201
LST	0.155
Road to Fire Distance	0.014
GEOLOGY	0.013
GEOMORPHOLOGY	0.02
ELEVATION	0.03
ASPECT	0.128
SLOPE	0.052

Now, the sum of the normalized weights i.e. $\sum W$ gave the sum value 1. A slight difference in the weightage of the factors from the weightage obtained by applying AHP was observed. Hence Fuzzy AHP was used to reduce the fuzziness in the decision-making process in the comparison matrix of AHP which helped to get a more accurate result. Now according to the normalized weights, ranks were given to the factors (Table 12).

C. Weighted Overlay (WO) for FAHP-Rated Factors

The weighted overlay method encrusts information based on factor layers to get a composite result. To provide a single, integrated analysis, it weighs each data layer according to its relative value and these weighted layers are then superimposed (Alharbi, 2024; Merchán et al., 2023). Applying the weighted overlay analysis involves overlapping all the GIS thematic layers and multiplying the weight value by each raster's cell value in the model builder (Hassan et al., 2020). Finally, a forest fire risk map was generated using weighted overlay analysis and the weight values obtained during the FAHP rating-weighting (Fig. 9).

Table 12. Ranks and Weightage of Factors using FAHP

Factors	Normalized Weights (W)	Ranks
LULC	0.082	5
NDVI	0.305	1
NDMI	0.201	2
LST	0.155	3
Road to Fire Distance	0.014	9
GEOLOGY	0.013	10
GEOMORPHOLOGY	0.02	8
ELEVATION	0.03	7
ASPECT	0.128	4
SLOPE	0.052	6

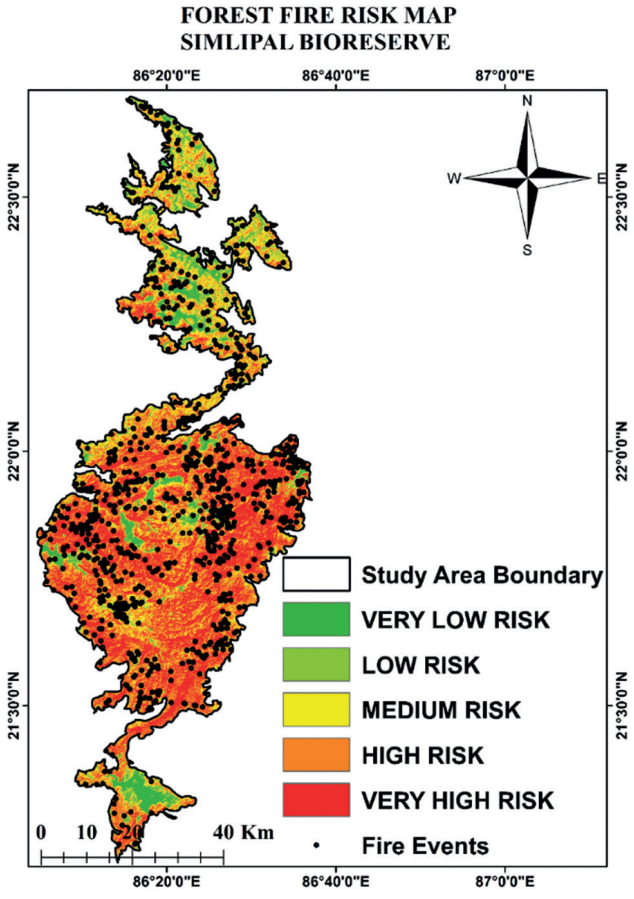

Figure 9. Forest fire risk map of the Similipal Biosphere Reserve generated using the Fuzzy Analytic Hierarchy Process (FAHP), providing refined susceptibility zoning

Mathematically,

$$\text{Index Map} = F1 * \text{Weightage} + F2 * \text{Weightage} + F3 * \text{Weightage} + F4 * \text{Weightage} + F5 * \text{Weightage} + F6 * \text{Weightage} + F7 * \text{Weightage} + F8 * \text{Weightage} + F9\ \text{Weightage} + F10 * \text{Weightage} \quad \text{eq. 15}$$

Here in this study, F1, F2, F3, F4, F5, F6, F7, F8, F9, and F10 indicate the factor maps i.e. LULC map, NDVI map, NDMI map, LST map, road to fire distance map, geology map, geomorphology map, elevation map, aspect map, and slope map respectively.

Following the creation and categorization of the forest fire risk maps, a unique map known as the burn severity map (Fig. 10) was produced using the annual fire data of the year 2021, which indicated the level of damage experienced in the study area due to previous extreme forest fire events.

To generate the burn severity, the following formula was used:

$$Burn\ Severity = \frac{NIR - SWIR}{NIR + SWIR}$$

where NIR = Near Infrared Band,
SWIR = Short Wave Infrared Band.

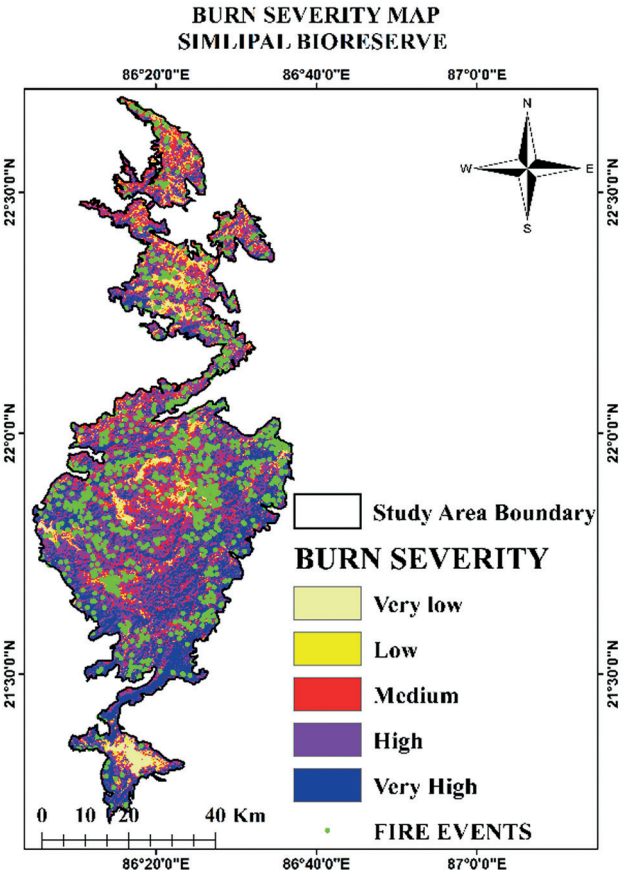

Figure 10. Burn Severity Map

A correlation between NDVI-burn severity and NDMI-burn severity was analysed using two scatter correlation graphs (Fig. 11 and Fig. 12), and they indicated a positive correlation; hence increase in vegetative cover increased burn severity, and also an increase in moisture index in the study area indicated an increase in vegetation cover, and hence the burn severity also increased.

The forest fire risk maps generated by applying AHP (Fig. 8) and FAHP (Fig. 9) delineate the land surface under very high risk to very low risk towards forest fire. The forest fire risk map generated using AHP indicates that out of the total AOI, 866 km^2 area extent is under a very high-risk zone that comprises around 25.21% of the total study area. The forest fire risk map generated by FAHP indicates that out of the total area, 1058 km^2 is under a very high-risk zone that comprises 30.79% of the total area. The historical fire events data aligns with the areas that are labelled as very high-risk zones for forest fire when the MODIS data is plotted with the index maps for the accuracy check.

Analysing the final risk maps also indicates that the areas that are under high risk are often associated with high vegetation, which is also associated with an increased amount of moisture; hence, it can be seen that the areas with high vegetation indicated by the NDVI map have a resemblance to the areas with high moisture content indicated in the NDMI map. A large amount of vegetation also creates a huge amount of debris, making such areas susceptible to debris flow and landslides due to the introduction of the rainy season soon after the forest fires. During forest fire, as the temperature increases the oils, resins, and fats stored in the plants get evaporated into the atmosphere and they also penetrate the ground and create a hydrophobic layer [https://www.csus.edu/indiv/k/kusnickj/geology140/fire.html] that induces slope instability as soon as there is rain as the run off will increase and the water won't be able to penetrate the soil due to the presence of the hydrophobic layer. With this high runoff speed, the soil along with the debris created during the forest fire will start to flow and the accumulation of such flow can lead to debris floods. Such instability in slope can also induce a landslide, as the rain after the forest fire makes a favourable condition that can induce slope instability on highly inclined slopes, loss of vegetation, high runoff speed etc. Tables 13 and 14 present the area occupied by zones that were categorized according to their risk level to forest fire in the Forest Fire Risk Map, applying the AHP model (Fig. 8) and FAHP model (Fig. 9), respectively.

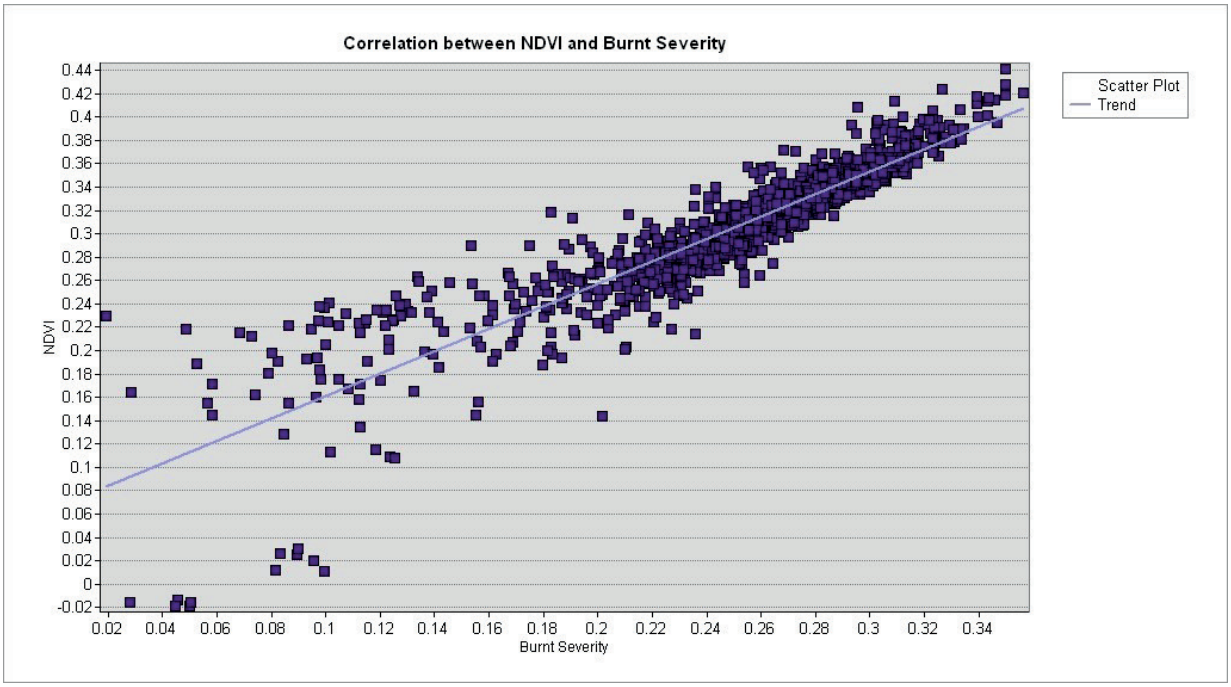

Figure 11. Correlation Between NDVI and Burn Severity

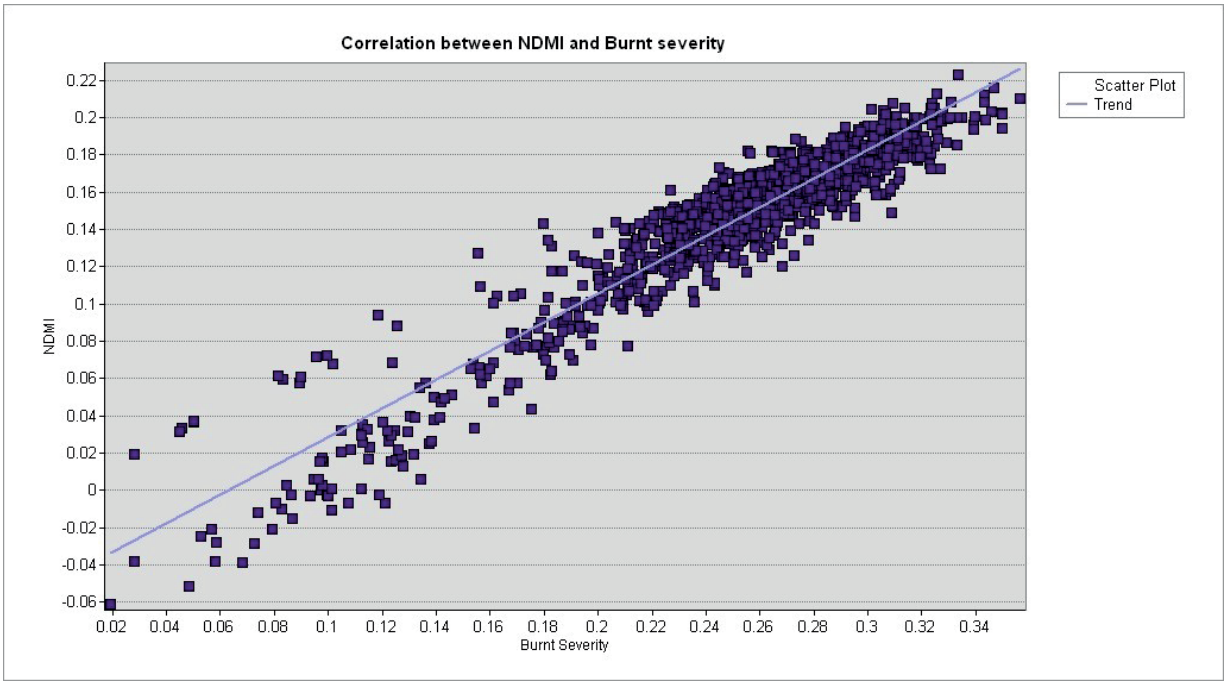

Figure 12. Correlation between NDMI and Burn Severity

Table 13. Area under different zones according to FFRM applying AHP

Zones	Area (km^2)
Very Low Risk	213
Low Risk	395
Medium Risk	845
High Risk	1116
Very High Risk	866

Table 14. Area under different zones according to FFRM applying FAHP

Zones	Area (km^2)
Very Low Risk	202
Low Risk	296
Medium Risk	722
High Risk	1158
Very High Risk	1058

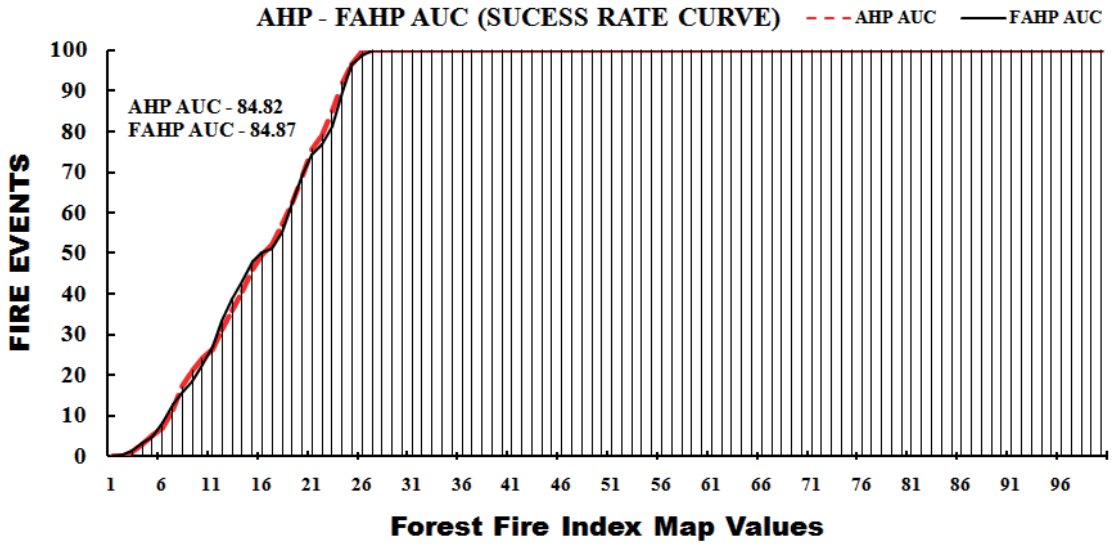

Figure 13. Success Rate Curve for index maps based on AHP and FAHP models

4.3. Validation

To validate the performance of AHP and FAHP-based index maps an accuracy check was run using the area under the curve (Success Rate Curve) method (Fig. 13), giving a value of 84.82 and 84.87 for AHP and FAHP-based models, respectively. The results show almost similar success rates for AHP and FAHP models and indicate good user consistency in choosing the rating of the criteria and the sub-criteria. Appendix 2 shows the pixel coverage of burn severity in various parts of the study area with respect to the pixel distribution in forest fire risk classes of AHP and FAHP-based maps.

5. Conclusions

Statistics from this study revealed that more than 50% of the total study area falls under high and very high risk of forest fires. This emphasizes the vulnerability towards forest fires in the study area which pose a serious threat to its biodiversity and environment. The fact is that the 2021 forest fire brought into evidence the biggest natural threat prevailing in this region that can lead to the loss of ecological habitat to many species if proper steps to mitigate the risk are not taken.

This study presents the methodology and techniques for assessing and mapping the areas at risk to future forest fires. The application of the Analytic Hierarchy Process (AHP) and Fuzzy AHP indicated the important factors that raise the probability of forest fires in this area the study has also shown how to extract forest fire risk information from satellite images and when combined with historical forest fire event data (such as MODIS fire data used) it can demarcate the zones of forest fire risk with reliable results.

The study also indicated that the fire events in the forest reserve region take place between January and April, inferring that the area is susceptible to forest fire during the pre-monsoon season, which indicates that the dry season results in the accumulation of dead leaves, branches, and trees, which act as fuel to the fire. These factors should be kept in mind, and regular surveillance by the fire department and forest department must be carried out to minimize the dry season products, especially in area that has maximum natural vegetation cover.

While both methods inferred NDVI and NDMI as dominant drivers of forest fires, FAHP resulted in relatively higher normalized weights compared to AHP. This suggests that the uncertainty in judgment accounted for, vegetation density, and moisture index were greater as controlling factors of fire risk in the Similipal Bioreserve. Whereas, the factors such as slope and aspect resulted in minor weightage shifts between AHP and FAHP, indicating topographic controls as secondary factors to fuel the forest fire.

Furthermore, this study can be taken as a stepping stone to research the post-fire debris flow hazards using the slope maps and fire-risk zones mapped from the present study. Looking at the recent global climate change and extreme temperatures in many parts of India, if the forest fire events increase in various regions, it will also increase the requirement for the assessment of debris-flow hazards through additional field-verified inventories of postfire rainfall-triggered events. Such studies are required for informed decision-making in disaster-prone areas.

Statements and Declarations:
The authors have received no funding for the research work and have submitted the article with mutual consent. The authors also declare no competing interests related to the work. No potential conflict of interest was reported by the author(s).

Data availability statement:
The data used in this work is freely available, and anyone can use it by downloading it from the sources. Further data may be shared upon reasonable request.

References

Abedi Gheshlaghi, H., Feizizadeh, B., & Blaschke, T., 2020, GIS-based forest fire risk mapping using the analytical network process and fuzzy logic. Journal of Environmental Planning and Management 63(3): 481–499.

Ahmad, F., Goparaju, L., & Qayum, A., 2018, Himalayan forest fire characterization in relation to topography, socio-economy, and meteorological parameters in Arunachal Pradesh, India. Spatial Information Research 26(3): 305–315.

Alharbi, T., 2024, A Weighted Overlay Analysis for Assessing Urban Flood Risks in Arid Lands: A Case Study of Riyadh, Saudi Arabia. Water 16(3), 397.

Andreae, M.O., Rosenfeld, D., Artaxo, P., Costa, A.A., Frank, G.P., Longo, K.M., & Silva-Dias, M.A.F.D., 2004, Smoking rain clouds over the Amazon. Science 303(5662): 1337–1342.

Araújo Santos, L.M., Correia, A.J., & Coelho, P.A., 2020, Post-wildfire slope stability effects and mitigation: A case study from hilly terrains with unmanaged forest. SN Applied Sciences 2(11), 1883.

Arca, D., Hacısalihoğlu, M., & Kutoğlu, Ş.H., 2020, Producing a forest fire susceptibility map via multi-criteria decision analysis and frequency ratio methods. Natural Hazards 104: 73–89.

Basak, D., Bose, A., Roy, S., & Chowdhury, I.R., 2023, Understanding the forest cover dynamics and its health status using GIS-based analytical hierarchy process: a study from Alipurduar district, West Bengal, India. In Water, land, and forest susceptibility and sustainability, pp. 475–508. Elsevier.

Bobsien, A, & Hoffmann, E., 1998, Plantations and Forest Fires in Indonesia. Presented at the 11th International NGO Forum on Indonesian Development Conference on Democratization in the Era of Globalization, May 4–6, 1998, Bonn, Germany.

Boender, C.G.E., De Graan, J.G., & Lootsma, F., 1989, Multi-criteria decision analysis with fuzzy pairwise comparisons. Fuzzy sets and Systems 29(2): 133–143.

Bourenane, H., Bouhadad, Y., Guettouche, M.S., & Braham, M., 2015, GIS-based landslide susceptibility zonation using bivariate statistical and expert approaches in the city of Constantine (Northeast Algeria). Bulletin of Engineering Geology and the Environment 74: 337–355.

Bouyssou, D., 2000, Evaluation and decision models: a critical perspective (Vol. 32). Springer Science & Business Media.

Bowman, D.M., Williamson, G.J., Gibson, R.K., Bradstock, R.A., & Keenan, R.J., 2021, The severity and extent of the Australia 2019–20 Eucalyptus forest fires are not the legacy of forest management. Nature Ecology & Evolution 5(7): 1003–1010.

Buckley, J.J., 1985a, Fuzzy hierarchical analysis. Fuzzy sets and systems 17(3): 233–247.

Buckley, J.J., 1985b, Ranking alternatives using fuzzy numbers. Fuzzy sets and systems 15(1): 21–31.

Cellek, S., 2021, The effect of aspect on landslide and its relationship with other parameters. In Landslides. IntechOpen.

Chand, T.K., Badarinath, K.V.S., Prasad, V.K., Murthy, M.S.R., Elvidge, C.D., & Tuttle, B.T., 2006, Monitoring forest fires over the Indian region using Defense Meteorological Satellite Program-Operational Linescan System nighttime satellite data. Remote Sensing of Environment 103(2): 165–178.

Chavan, M., Das, K.K., & Suryawanshi, R., 2012, Forest fire risk zonation using remote sensing and GIS in Huynial watershed, Tehri Garhwal district, UA. Int J Basic Appl Res. 2(7): 6–12.

Chen, S.C., Chang, C.C., Chan, H.C., Huang, L.M., & Lin, L.L., 2013, Modeling Typhoon Event-Induced Landslides Using GIS-Based Logistic Regression: A Case Study of Alishan Forestry Railway, Taiwan. Mathematical Problems in Engineering 2013(1), 728304.

Chowdhury, E.H., & Hassan, Q.K., 2013, Use of remote sensing-derived variables in developing a forest fire danger forecasting system. Natural Hazards 67: 321–334.

Chowdhury, E.H., & Hassan, Q.K., 2015, Operational perspective of remote sensing-based forest fire danger forecasting systems. ISPRS Journal of Photogrammetry and Remote Sensing 104: 224–236.

Chuvieco, E., & Congalton, R.G., 1989, Application of remote sensing and geographic information systems to forest fire hazard mapping. Remote Sensing of Environment 29(2): 147–159.

Dash, M., & Behera, B., 2018, Biodiversity conservation, relocation and socio-economic consequences: A case study of Similipal Tiger Reserve, India. Land Use Policy 78: 327–337.

Dhar, T., Bhatta, B., & Aravindan, S., 2023, Forest fire occurrence, distribution and risk mapping using geoinformation technology: A case study in the sub-

tropical forest of the Meghalaya, India. Remote Sensing Applications: Society and Environment 29, 100883.

Erten, E., Kurgun, V., & Musaoglu, N., 2004(July), Forest fire risk zone mapping from satellite imagery and GIS: a case study. In XXth Congress of the International Society for Photogrammetry and Remote Sensing, Istanbul, Turkey, pp. 222–230.

Esteves, T.C.J., Kirkby, M.J., Shakesby, R.A., Ferreira, A.J.D., Soares, J.A.A., Irvine, B.J., … & Carreiras, M.A., 2012, Mitigating land degradation caused by wildfire: Application of the PESERA model to fire-affected sites in central Portugal. Geoderma 191: 40–50.

Geiger, R., Aron, R.H., & Todhunter, P., 2009, The climate near the ground . Rowman & Littlefield.

Ghorbanzadeh, O., Valizadeh Kamran, K., Blaschke, T., Aryal, J., Naboureh, A., Einali, J., & Bian, J., 2019, Spatial prediction of wildfire susceptibility using field survey GPS data and machine learning approaches. Fire: 2(3), 43.

Giglio, L., Van der Werf, G.R., Randerson, J.T., Collatz, G.J., & Kasibhatla, P., 2006, Global estimation of burned area using MODIS active fire observations. Atmospheric Chemistry and Physics 6(4): 957–974.

Gong, J., Jin, T., Cao, E., Wang, S., & Yan, L., 2022, Is ecological vulnerability assessment based on the VSD model and AHP-Entropy method useful for loessial forest landscape protection and adaptative management? A case study of Ziwuling Mountain Region, China. Ecological Indicators 143, 109379.

Hadji, R., Chouabi, A., Gadri, L., Raïs, K., Hamed, Y., & Boumazbeur, A., 2016, Application of linear indexing model and GIS techniques for the slope movement susceptibility modeling in Bousselam upstream basin, Northeast Algeria. Arabian Journal of Geosciences 9: 1–18.

Hassan, I., Javed, M.A., Asif, M., Luqman, M., Ahmad, S.R., Ahmad, A., … & Hussain, B., 2020, Weighted overlay based land suitability analysis of agricultural land in Azad Jammu and Kashmir using GIS and AHP. Pakistan Journal of Agricultural Sciences 57(6): 1509–1519.

Huang, S., Tang, L., Hupy, J.P., Wang, Y., & Shao, G., 2021, A commentary review on the use of normalized difference vegetation index (NDVI) in the era of popular remote sensing. Journal of Forestry Research 32(1): 1–6.

Jain, A., Ravan, S.A., Singh, R.K., Das, K.K., & Roy, P.S., 1996, Forest fire risk modelling using remote sensing and geographic information system. Current Science 70: 928–933.

Jaiswal, R.K., Mukherjee, S., Raju, K.D., & Saxena, R., 2002, Forest fire risk zone mapping from satellite imagery and GIS. International journal of applied earth observation and geoinformation 4(1): 1–10.

Jolly, W.M., Cochrane, M.A., Freeborn, P.H., Holden, Z. A.,Brown, T.J., Williamson, G.J., & Bowman, D.M., 2015, Climate-induced variations in global wildfire danger from 1979 to 2013. Nature Communications 6(1), 7537.

Kaufman, Y.J., Justice, C.O., Flynn, L.P., Kendall, J.D., Prins, E.M., Giglio, L., & Setzer, A.W., 1998, Potential global fire monitoring from EOS-MODIS. Journal of Geophysical Research: Atmospheres 103(D24): 32215–32238.

Keenan, R.J., 2015, Climate change impacts and adaptation in forest management: a review. Annals of Forest Science 72: 145–167.

Kriegler, F.J., 1969, Preprocessing transformations and their effects on multispectral recognition. In Proceedings of the Sixth International Symposium on Remote Sensing of Environment, pp. 97–131.

Lamat, R., Kumar, M., Kundu, A., & Lal, D., 2021, Forest fire risk mapping using analytical hierarchy process (AHP) and earth observation datasets: A case study in the mountainous terrain of Northeast India. SN Applied Sciences 3(4), 425.

Lee, S., 2005, Application of logistic regression model and its validation for landslide susceptibility mapping using GIS and remote sensing data. International Journal of Remote Sensing 26(7): 1477–1491.

Loboda, T.V., & Csiszar, I.A., 2007, Reconstruction of fire spread within wildland fire events in Northern Eurasia from the MODIS active fire product. Global and Planetary Change 56(3–4): 258–273.

Lootsma, F.A., 2013, Fuzzy logic for planning and decision making (Vol. 8). Springer Science & Business Media.

Mahajan, A.K., Sharma, S., Patial, S., Sharma, H., Pandey, D.D., & Negi, S., 2022, A brief address of the causal factors, mechanisms, and the effects of a major landslide in Kangra valley, North-Western Himalaya, India. Arabian Journal of Geosciences 15(9), 925.

Matin, M.A., Chitale, V.S., Murthy, M.S., Uddin, K., Bajracharya, B., & Pradhan, S., 2017, Understanding forest fire patterns and risk in Nepal using remote sensing, geographic information system and historical fire data. International Journal of Wildland Fire 26(4): 276–286.

Merchán, L., Martínez-Graña, A., Nieto, C.E., Criado, M., & Cabero, T., 2023, Characterization of the susceptibility to slope movements in the Arribes del Duero Natural Park (Spain). Land 12(8), 1513.

Middendorp, R.S., Vlam, M., Rebel, K.T., Baker, P.J., Bunyavejchewin, S., & Zuidema, P.A., 2013, Disturbance history of a seasonal tropical forest in western Thailand: a spatial dendroecological analysis. Biotropica 45(5): 578–586.

Moayedi, H., & Khasmakhi, M.A.S.A., 2023, Wildfire susceptibility mapping using two empowered machine

learning algorithms. Stochastic Environmental Research and Risk Assessment 37(1): 49–72.

Mutthulakshmi, K., Wee, M.R.E., Wong, Y.C.K., Lai, J.W., Koh, J.M., Acharya, U.R., & Cheong, K.H., 2020, Simulating forest fire spread and fire-fighting using cellular automata. Chinese Journal of Physics 65: 642–650.

Nunes, A.N., & Lourenço, L., 2017, Increased vulnerability to wildfires and post fire hydro-geomorphic processes in Portuguese mountain regions: what has changed?. Open Agriculture 2(1): 70–82.

Nur, A.S., Kim, Y.J., Lee, J.H., & Lee, C.W., 2023, Spatial prediction of wildfire susceptibility using hybrid machine learning models based on support vector regression in Sydney, Australia. Remote Sensing 15(3), 760.

Nuthammachot, N., & Stratoulias, D., 2021, A GIS-and AHP-based approach to map fire risk: a case study of Kuan Kreng peat swamp forest, Thailand. Geocarto International 36(2): 212–225.

Özdağoğlu, A., & Özdağoğlu, G., 2007, Comparison of AHP and fuzzy AHP for the multi-criteria decision making processes with linguistic evaluations. İstanbul Ticaret Üniversitesi Fen Bilimleri Dergisi 6(11): 65–85.

Oskouei1 E.A., Shobairi S.O.R., Hadis Sadeghi, Shokouhi M., Fatahi E., Khazanedari L., Lingxiao S., Haiyan Z., Chunlan L., Jing H., & Ayombekov O., 2024, Spatial and temporal monitoring of wildfires in Golestan province using remote sensing data. Ecological Questions 35(3): 17–32

Pandey, K., & Ghosh, S.K., 2018, Modeling of parameters for forest fire risk zone mapping. The international archives of the photogrammetry, remote sensing and spatial information sciences 42, 299–304.

Panwar V.K., & Chaudhry P., 2019, Major challenges and issues related to wildlife management in Kanha National Park, India. Ecological Questions 30(3): 79–86.

Pereira, A.A., Pereira, J.M., Libonati, R., Oom, D., Setzer, A.W., Morelli, F., … & De Carvalho, L.M.T., 2017, Burned area mapping in the Brazilian Savanna using a one-class support vector machine trained by active fires. Remote Sensing 9(11), 1161.

Potić, I.M., Ćurčić, N.B., Potić, M.M., Radovanović, M.M., & Tretiakova, T.N., 2017, Remote sensing role in environmental stress analysis: East Serbia wildfires case study (2007–2017). Journal of the Geographical Institute" Jovan Cvijic", SASA 67(3): 249–264.

Pourghasemi, H.R., Beheshtirad, M., & Pradhan, B., 2016, A comparative assessment of prediction capabilities of modified analytical hierarchy process (M-AHP) and Mamdani fuzzy logic models using Netcad-GIS for forest fire susceptibility mapping. Geomatics, Natural Hazards and Risk 7(2): 861–885.

Prakasam, C., 2010, Land use and land cover change detection through remote sensing approach: A case study of Kodaikanal Taluk, Tamil Nadu. International Journal of Geomatics and Geosciences 1(2), 150.

Ramanathan, V.C.P.J., Crutzen, P.J., Kiehl, J.T., & Rosenfeld, D., 2001, Aerosols, climate, and the hydrological cycle. Science 294(5549): 2119–2124.

Rawat, J.S., & Kumar, M., 2015, Monitoring land use/cover change using remote sensing and GIS techniques: A case study of Hawalbagh block, district Almora, Uttarakhand, India. The Egyptian Journal of Remote Sensing and Space Science 18(1): 77–84.

Reis, S., 2008, Analyzing land use/land cover changes using remote sensing and GIS in Rize, North-East Turkey. Sensors 8(10): 6188–6202.

Ribeiro, R.A., 1996, Fuzzy multiple attribute decision making: a review and new preference elicitation techniques. Fuzzy Sets and Systems 78(2): 155–181.

Roy, D.P., Lewis, P.E., & Justice, C.O., 2002, Burned area mapping using multi-temporal moderate spatial resolution data—A bi-directional reflectance model-based expectation approach. Remote Sensing of Environment 83(1–2): 263–286.

Saaty, R.W., 1987, The analytic hierarchy process—what it is and how it is used. Mathematical Modelling 9(3–5): 161–176.

Saini, S.S., & Kaushik, S.P., 2012, Risk and vulnerability assessment of flood hazard in part of Ghaggar Basin: A case study of Guhla block, Kaithal, Haryana, India. International Journal of Geomatics and Geosciences 3(1): 42–54.

Sankey, T.T., Tango, L., Tatum, J., & Sankey, J.B., 2024, Forest fire, thinning, and flood in wildland-urban interface: UAV and lidar-based estimate of natural disaster impacts. Landscape Ecology 39(3), 58.

Sarkis, J., & Talluri, S., 2004, Evaluating and selecting e-commerce software and communication systems for a supply chain. European Journal of Operational Research 159(2): 318–329.

Seyam, M.M.H., Haque, M.R., & Rahman, M.M., 2023, Identifying the land use land cover (LULC) changes using remote sensing and GIS approach: A case study at Bhaluka in Mymensingh, Bangladesh. Case Studies in Chemical and Environmental Engineering 7, 100293.

Shi, C., & Zhang, F., 2023, A forest fire susceptibility modelling approach based on integration of machine learning algorithms. Forests 14(7), 1506.

Simioni, G., Marie, G., Davi, H., Martin-St Paul, N., & Huc, R., 2020, Natural forest dynamics have more influence than climate change on the net ecosystem production of a mixed Mediterranean forest. Ecological Modelling 416, 108921.

Singh, Shipra, 2018, Understanding the role of slope aspect in shaping the vegetation attributes and soil properties in Montane ecosystems. Tropical Ecology 59(3): 417–430.

Singha, C., Swain, K.C., Moghimi, A., Foroughnia, F., & Swain, S.K., 2024, Integrating geospatial, remote sensing, and machine learning for climate-induced forest fire susceptibility mapping in Similipal Tiger Reserve, India. Forest Ecology and Management 555, 121729.

Taloor, A.K., Manhas, D.S., & Kothyari, G.C., 2021, Retrieval of land surface temperature, normalized difference moisture index, normalized difference water index of the Ravi basin using Landsat data. Applied Computing and Geosciences 9, 100051.

Tamrakar, Y., Das, I. C., & Sharma, S. (2024). Machine learning for improved drought forecasting in Chhattisgarh India: a statistical evaluation. Discover Geoscience, 2(1), 84.

Tanoli, J.I., Ningsheng, C., Regmi, A.D., & Jun, L., 2017, Spatial distribution analysis and susceptibility mapping of landslides triggered before and after Mw7. 8 Gorkha earthquake along Upper Bhote Koshi, Nepal. Arabian Journal of Geosciences 10: 1–24.

Teke, A., & Kavzoglu, T., 2025, Explainable Artificial Intelligence to Unveil Intrinsic Characteristics of Conditioning Factors Governing Forest Fire Susceptibility. The International Archives of the Photogrammetry, Remote Sensing and Spatial Information Sciences 48: 281–287.

Tiwari, A., Shoab, M., & Dixit, A., 2021, GIS-based forest fire susceptibility modeling in Pauri Garhwal, India: a comparative assessment of frequency ratio, analytic hierarchy process and fuzzy modeling techniques. Natural Hazards 105(2): 1189–1230.

Van Hoang, T., Chou, T.Y., Fang, Y.M., Nguyen, N.T., Nguyen, Q.H., Xuan Canh, P., … & Meadows, M.E., 2020, Mapping forest fire risk and development of early warning system for NW Vietnam using AHP and MCA/GIS methods. Applied Sciences 10(12), 4348.

Van Laarhoven, P.J., & Pedrycz, W., 1983, A fuzzy extension of Saaty's priority theory. Fuzzy Sets and Systems 11(1–3): 229–241.

Vlassova, L., Pérez-Cabello, F., Mimbrero, M.R., Llovería, R.M., & García-Martín, A., 2014, Analysis of the relationship between land surface temperature and wildfire severity in a series of Landsat images. Remote Sensing 6(7): 6136–6162.

Warren, R.J., 2008, Mechanisms driving understory evergreen herb distributions across slope aspects: as derived from landscape position. Plant Ecology 198: 297–308.

Yue, X., Mickley, L.J., Logan, J.A., & Kaplan, J.O., 2013. Ensemble projections of wildfire activity and carbonaceous aerosol concentrations over the western United States in the mid-21st century. Atmospheric Environment, 77, 767–780.

Zêzere, J.L., Vaz, T., Pereira, S., Oliveira, S.C., Marques, R., & Garcia, R.A., 2015, Rainfall thresholds for landslide activity in Portugal: a state of the art. Environmental Earth Sciences 73: 2917–2936.

Zhuang, J., Cui, P., Wang, G., Chen, X., Iqbal, J., & Guo, X., 2015, Rainfall thresholds for the occurrence of debris flows in the Jiangjia Gully, Yunnan Province, China. Engineering Geology 195: 335–346.